JCTC Journal of Chemical Theory and Computation

On the Angular Dependence of the Vicinal Fluorine−Fluorine Coupling Constant in 1,2-Difluoroethane: Deviation from a Karplus-like Shape

Patricio F. Provasi*

Department of Physics, University of Northeastern, Av. Libertad 5500, W 3404 AAS Corrientes, Argentina

Stephan P. A. Sauer†

Department of Chemistry, University of Copenhagen, Universitetsparken 5, DK-2100 Copenhagen Ø, Denmark

Received March 20, 2006

Abstract: The angular dependence of the vicinal fluorine−fluorine coupling constant, $^3J_{FF}$, for 1,2-difluoroethane has been investigated with several polarization propagator methods. $^3J_{FF}$ and its four Ramsey contributions were calculated using the random phase approximation (RPA), its multiconfigurational generalization, and both second-order polarization propagator approximations (SOPPA and SOPPA(CCSD)), using locally dense basis sets. The geometries were optimized for each dihedral angle at the level of density functional theory using the B3LYP functional and fourth-order Møller−Plesset perturbation theory. The resulting coupling constant curves were fitted to a cosine series with 8 coefficients. Our results are compared with those obtained previously and values estimated from experiment. It is found that the inclusion of electron correlation in the calculation of $^3J_{FF}$ reduces the absolute values. This is mainly due to changes in the FC contribution, which for dihedral angles around the trans conformation even changes its sign. This sign change is responsible for the breakdown of the Karplus-like curve.

1. Introduction

The sensitivity of indirect spin−spin coupling constants (J) to structural changes is a powerful tool for determination of molecular structures and conformations. As an example we can mention the dependence of J on bond or dihedral angles which has been the object of many studies (see e.g., the review by Contreras and Peralta[1] and references therein). In particular, the study of the dependence of coupling constants on torsion angles became an important issue after Karplus presented his already classical equation.[2] In recent years some new attempts were made to explain the origin of this behavior.[3]

Coupling constants involving fluorine atoms have recently attracted much interest,[4−12] due to the important biological activity of fluorinated organic compounds,[13] their use in medicine for NMR imaging techniques,[14] their possible use in quantum computers,[15] and their unusual behavior such as e.g. long-range through-bond[10] and through-space couplings.[5,12] Another example for the unusual behavior of fluorine coupling constants is the dependence of vicinal fluorine−fluorine coupling constant $^3J_{FF}$ on the dihedral angle in 1,2-difluoroethane[7,9,16] which differs greatly from the usual Karplus curve as found e.g. for the vicinal proton−proton coupling in ethane.[17,18]

Kurtkaya et al.[7] have calculated $^3J_{FF}$ using density functional theory (DFT)[19] with the B3LYP functional[20] and the 6-311G(d,p) basis set.[21] Their geometries were optimized at the same level of theory for each fixed F−C−C−F dihedral angle. They analyzed the dominating Fermi contact contribu-

* Corresponding author e-mail: patricio@unne.edu.ar.

† Present address: Max-Planck-Institut für Kohlenforschung, Kaiser Wilhelm-Platz 1, D-45470 Mülheim an der Ruhr, Germany.

10.1021/ct6000973 CCC: $33.50
Published on Web 06/01/2006

tion to $^3J_{FF}$ in 1,2-difluoroethane in terms of the carbon−fluorine bond orbitals and the lone pairs orbitals of fluorine. However, their calculated vicinal coupling for the trans conformation is not in agreement with the known experimental value, which is not surprising since the B3LYP as well as most of the current functionals were shown[5,6,8,18,22] to have problems reproducing coupling constants that involve at least one fluorine atom.

More recently, San Fabián and Westra Hoekzema[9] presented Karplus curves for $^3J_{FF}$ in 1,2-difluoroethane calculated with the multiconfigurational random phase approximation (MCRPA)[23,24] with various restricted active space self-consistent field (RASSCF) wave functions,[25] the second-order polarization propagator approximation (SOPPA),[26,27] and DFT using the BLYP functional. Their geometries were either optimized at the B3LYP level using the cc-pVTZ basis set[28] for a fixed F−C−C−F dihedral angle or were kept fixed during rotation at the values of a standard C−C bond length and tetrahedral bond angles. They fitted their curves to truncated Fourier series in the torsion angle ϕ and found that the number of Fourier coefficients necessary for a proper representation of the Karplus curve is too large for an empirical parametrization based on experimental coupling constants. They conclude that the missing data have to be provided by high accuracy calculations. With respect to the different correlated methods, they find that SOPPA gives in general the best agreement with experimental values, but that important differences remain in particular for some of the Fourier coefficients and for the trans coupling, for which the largest differences between the various calculations are observed. Furthermore equally large changes in the Fourier coefficients are observed between the SOPPA calculations with standard and optimized geometries, and the authors concluded that good geometries must be used in the calculation of these couplings.

Several years ago a modification of the SOPPA method was introduced in which the Møller−Plesset correlation coefficients are replaced by the corresponding coupled cluster singles and doubles amplitudes in the SOPPA equations. This second-order polarization propagator approximation with coupled cluster singles and doubles amplitudes—SOPPA-(CCSD)[29]—called method was shown to give more accurate coupling constants than SOPPA.[8,17,27,30−33] Furthermore tiny changes in the coupling constants such as temperature dependence and isotope effects, which originate in the geometry dependence of the coupling constants, could quantitatively be reproduced by SOPPA(CCSD) calculations.[32,34]

In the present work we have therefore studied the large correlation and geometry effects on the vicinal fluorine−fluorine couplings in 1,2-difluoroethene and its four contributions using SOPPA(CCSD). Geometries optimized at the level of DFT/B3LYP and fourth-order Møller−Plesset perturbation theory (MP4)[35] using the 6-311G(d,p) basis set were employed in the calculations. In addition, calculations at the level of the random phase approximation (RPA),[36] the MCRPA with various RASSCF wave functions, and SOPPA were performed.

The paper is organized as follows: the next section gives a short review of the theory of spin−spin coupling constants and the quantum chemical methods for the calculation of *J*. The details of our calculations are explained in section 3. Section 4 is devoted to the presentation and discussion of our results, and finally in section 5 our conclusions are presented.

2. Theory

Ramsey[37] has explained the total nonrelativistic indirect nuclear spin−spin coupling constant between nuclei M and N as the sum of four contributions. They are the diamagnetic nuclear spin−electronic orbital (DSO), the paramagnetic nuclear spin−electronic orbital (PSO), nuclear spin−electronic spin dipolar (SD), and the Fermi contact (FC) contributions

$$J_{MN}^{Tot} = J_{MN}^{DSO} + J_{MN}^{PSO} + J_{MN}^{SD} + J_{MN}^{FC} \tag{1}$$

where the FC and SD terms account for the interaction of the nuclear spin with the spins of the electrons, and the PSO and DSO terms account for the interaction of the nuclear spin with the orbital angular momentum of the electrons.

The DSO contribution is a ground-state average value

$$J_{MN}^{DSO} = \frac{1}{3}\frac{\gamma_M\gamma_N}{h}\left(\frac{\mu_0}{4\pi}\right)^2\frac{e^2\hbar^2}{m_e}\sum_{\alpha=x,y,z}\left\langle\Psi_0\left|\sum_i\frac{\vec{r}_{iN}\cdot\vec{r}_{iM} - (\vec{r}_{iN})_\alpha(\vec{r}_{iM})_\alpha}{|\vec{r}_{iN}|^3|\vec{r}_{iM}|^3}\right|\Psi_0\right\rangle \tag{2}$$

although it can also be expressed in a form which involves excited states.[38]

The last three contributions can be expressed as a sum over excited states in the following way

$$J_{MN}^{A} = \sum_{\alpha=x,y,z}\frac{2}{3}\frac{\gamma_M\gamma_N}{h}\sum_{n\neq 0}\frac{\langle\Psi_0|(\hat{\vec{O}}_M^A)_\alpha|\Psi_n\rangle\langle\Psi_n|(\hat{\vec{O}}_N^A)_\alpha|\Psi_0\rangle}{E_0 - E_n} \tag{3}$$

where A = PSO, SD, FC. The explicit expressions of the above operators are

$$(\hat{\vec{O}}_M^{PSO})_\alpha = \frac{\mu_0}{4\pi}\frac{e\hbar}{m_e}\sum_i\frac{(\vec{l}_{iM})_\alpha}{r_{iM}^3} \tag{4}$$

$$(\hat{\vec{O}}_M^{FC})_\alpha = \frac{\mu_0}{4\pi}\frac{4\pi g_e e\hbar}{3m_e}\sum_i(\vec{s}_i)_\alpha\delta(\vec{r}_{iM}) \tag{5}$$

$$(\hat{\vec{O}}_M^{SD})_\alpha = \frac{\mu_0}{4\pi}\frac{g_e e\hbar}{2m_e}\sum_i\frac{3(\vec{s}_i\cdot\vec{r}_{iM})(\vec{r}_{iM})_\alpha - r_{iM}^2(\vec{s}_i)_\alpha}{r_{iM}^5} \tag{6}$$

The gyromagnetic ratio of nucleus M is γ_M, $\vec{r}_{iM} = \vec{r}_i - \vec{r}_M$ is the difference of the position vectors of electron *i* and nucleus M, $\vec{s}_i$ is the spin operator of electron *i*, $\vec{l}_{iM} = \vec{l}_i(\vec{R}_M)$ is the orbital angular momentum operator of electron *i* with respect to the position of nucleus M (in SI units), $\delta(x)$ is the

Dirac delta function, and all other symbols in eqs 1−6 have their usual meaning.[39]

The FC and SD contributions, that account for the interaction with the spin of the electrons, arise from the admixture of excited triplet states $|\Psi_n\rangle$ to the singlet ground state $|\Psi_0\rangle$, whereas the OP term only involves excited states $|\Psi_n\rangle$ of the same spin symmetry as the ground state $|\Psi_0\rangle$.

Using polarization propagator[40] or linear response function methods[24] all contributions to the coupling constants can be evaluated without explicit calculation of the excited states involved[41]

$$J^A_{MN} = -\begin{pmatrix} \langle\Psi_0 \mid [(\hat{\tilde{O}}^A_M)_\alpha, \hat{h}_i] \mid \Psi_0\rangle & \cdots \end{pmatrix} \begin{pmatrix} \langle\Psi_0 \mid [\hat{h}_i, [\hat{H}, \hat{h}_j]] \mid \Psi_0\rangle & \cdots \\ \vdots & \ddots \end{pmatrix}^{-1} \begin{pmatrix} \langle\Psi_0 \mid [\hat{h}_j, (\hat{\tilde{O}}^A_N)_\alpha] \mid \Psi_0\rangle \\ \vdots \end{pmatrix} \quad (7)$$

where $\hat{H}$ is the electronic Hamiltonian of the system, and $\{\hat{h}_i\}$ is a complete set of operators. Different approximate propagator methods can then be derived by truncating the set of operators $\{\hat{h}_i\}$ and approximating the exact ground-state wave function Ψ_0 using either variational or perturbational approaches. Examples for the former are the random phase approximation[36] or self-consistent field (SCF) linear response function[24] and its multiconfigurational generalization MCRPA,[23,24] where either only the molecular orbital coefficients or the molecular orbital coefficients and the determinant expansion coefficients are variationally optimized in the wave function Ψ_0. The set of operators $\{\hat{h}_i\}$ consists then correspondingly of either only orbital rotation operators or orbital rotation operators and state transfer operators. To treat dynamic correlation properly with MCPRA very large determinant expansions have to be included in the wave function, which makes high accuracy MCRPA calculations prohibitively expensive.

Alternatively, dynamic correlation can be treated by methods based on Møller−Plesset perturbation[42] such as SOPPA.[26,27] From the viewpoint of the perturbation theory the polarization propagator, eq 7, is evaluated to the first order in the fluctuation potential[43] in RPA. Furthermore a closer analysis of the terms entering the RPA matrices[44] shows that the ground state in RPA is correlated by the inclusion of doubly excited determinants. For this reason RPA or coupled Hartree−Fock is sometimes considered to be a correlated method[45] contrary to the uncoupled Hartree−Fock approach. In SOPPA the matrix elements in eq 7 are evaluated through second order in the fluctuation potential. If the Møller−Plesset perturbation theory correlation coefficients in the SOPPA equations are replaced with coupled cluster single and double (CCSD) amplitudes, one obtains the SOPPA(CCSD) method.[29]

The dihedral angle dependence of the vicinal fluorine−fluorine coupling constant is best represented by a truncated

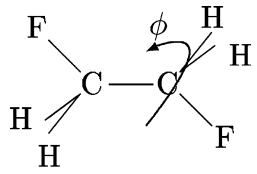

Figure 1. The optimization of structures was performed with the dihedral angle ϕ (∠F−C−C−F) fixed at 0°, 15°, 30°, 45°, 60°, 80°, 90°, 100°, 115°, 135°, 150°, 165°, and 180° [see ref 7].

Fourier series in the dihedral angle ϕ

$$^3J^{\mathrm{Tot}}_{\mathrm{F-F}}(\phi) = C_0 + C_1\cos(\phi) + C_2\cos(2\phi) + C_3\cos(3\phi) + C_4\cos(4\phi) + C_5\cos(5\phi) + C_6\cos(6\phi) + C_7\cos(7\phi) + \cdots \quad (8)$$

Truncation of this series after the $C_2\cos(2\phi)$ term gives the original equation by Karplus.[2]

3. Details of Calculations

Geometry Optimizations. All geometry optimizations were performed with the Gaussian 98 program[46] at the Hartree−Fock (HF), DFT-B3LYP,[20] MP2,[42] MP3, and full MP4[35] levels of theory using the 6-311G(d,p) basis set.[21] In all structures the dihedral angle ∠F−C−C−F was fixed to the values given in Figure 1 [see also ref 7]. The C and F 1s orbitals were kept frozen in the correlated calculations. The dihedral angle in the gauche conformation, i.e. the gauche angle, and the energy of the gauche conformation were obtained by fitting the rotamer energy curves with second-order splines.

***J*-Calculations.** All *J* calculations were performed with the 1.2 version of the Dalton program package.[47] Locally dense basis sets (LDBS)[11,48] were employed in order to keep the basis set size within the current limitations of the SOPPA implementation in the program. Hence, the aug-cc-pVTZ-J[31,49] basis set, which ensures a very good description of the FC term [see ref 31 and therein cited references], was used for the fluorine and carbon atoms which define the coupling pathway, whereas the cc-pVTZ[28] basis set was employed for all hydrogen atoms.

In the MCRPA calculations we tested two different RASSCF wave functions (RAS-A and RAS-B), which differ in the number of orbitals included in RAS3. In all cases the 1*s* molecular orbitals of carbon and fluorine were kept frozen, and the remaining occupied Hartree−Fock orbitals were included in RAS2. Single and double excitations were allowed from RAS2 into RAS3. The RASSCF wave functions could therefore be described as truncated configuration interaction singles and doubles (CISD) wave functions with optimized orbitals. The nomenclature used for the RAS wave functions is $^{\mathrm{inactive}}_{\mathrm{RAS1}}\mathrm{RAS}^{\mathrm{RAS2}}_{\mathrm{RAS3}}$, where *inactive*, RAS1, RAS2, and RAS3 are the total numbers of orbitals in these spaces, as all RASSCF calculations were run without the use of symmetry. The precise details of the two RASSCF wave functions are given in Table 1. Compared with the active spaces employed by San Fabián and Westra Hoekzema[9] we can see that our RAS-A is the same as R30, whereas RAS-B is larger than R45.

Table 1: Description of the RASSCF Wave Functions

label	active space[a,b]	N_{SD}[c]
RAS-A	$^{4}RAS^{13}_{13}$	14535
RAS-B	$^{4}RAS^{13}_{31}$	81810

[a] The nomenclature for the active spaces is $^{\text{inactive}}_{\text{RAS1}}\text{RAS}^{\text{RAS2}}_{\text{RAS3}}$, where *inactive*, RAS1, RAS2, and RAS3 are the total numbers of orbitals in these spaces, as all RASSCF calculations were run without the use of symmetry. [b] Only single and double excitations are allowed ($0 \rightarrow 2$). [c] Number of determinants in the wave function.

Table 2: Relative Energies in kJ/mol of the Cis, Trans, and Gauche Conformations of 1,2-Difluoroethane and the Dihedral Angle in the Gauche Conformation Obtained at the HF, DFT-B3LYP, MP2, MP3, and MP4 Levels of Theory with the 6-311G(d,p) Basis Set

	relative energies in kJ/mol			
method	cis	trans	gauche	dihedral angle gauche
HF	33.11	−0.66	0.0	69.962°
DFT-B3LYP	32.58	1.55	0.0	71.683°
MP2	34.13	1.13	0.0	69.639°
MP3	31.31	0.77	0.0	69.523°
MP4	32.56	0.76	0.0	69.442°

4. Results and Discussion

In this section, we first discuss the energies of the three conformations obtained at the HF, DFT-B3LYP, MP2, and MP4 levels. We discuss then the dependence of the $^{3}J_{FF}$ curves on the optimization of the geometries and the level of correlation included in the calculations. Finally, we compare our results with previous results and experimental values.

4.1. Rotamer Energies. A complete list of the HF, DFT-B3LYP, MP2, MP3, and MP4 energies for the optimized geometries is included in the Supporting Information.[50] In Table 2 we have collected the relative energies of the cis, trans, and gauche conformations of 1,2-difluoroethane as well as the values of the dihedral angle in the optimized gauche conformation, i.e. the gauche angle. All correlated methods predict the gauche conformation to be the absolute miminum in agreement with the spectroscopic findings,[51,52] whereas at the Hartree−Fock level the trans conformation is slightly lower in energy. B3LYP overestimates the relative energy of the trans conformation relative to the MP4 calculations, whereas both methods agree very well on the relative energy of the cis conformation. MP2, on the other hand, overestimates the relative energies of both rotamers. The shape of the rotamer potential energy curves are thus different in the various methods. This is also reflected in the predicted gauche angle which varies from 71.7° at B3LYP to 69.4° at MP4, i.e. by more than 2°. Compared with the uncorrelated HF calculation B3LYP predicts a larger angle, whereas all MP methods give smaller gauche angles.

4.2. Dependence of $^{3}J_{FF}$ on the Optimized Geometries. Vicinal fluorine−fluorine coupling constant curves $^{3}J_{FF}(\phi)$ have been calculated at the optimized MP4 and/or B3LYP geometries using RPA, RAS-A MCRPA, RAS-B MCRPA, SOPPA, and SOPPA(CCSD). The total coupling constants at both series of geometries obtained with the RAS-B wave function and at the SOPPA(CCSD) level are shown in Table 3. In the last three columns of Table 3 the changes in the total coupling constants and in the FC contribution (only at SOPPA(CCSD) level) due to the changes in the optimized geometries are given as well. Tables with the results for all four Ramsey components obtained with the four methods are given in the Supporting Information.[50]

The effect of the changes in the geometry is largest around the cis conformation with ∼1.5 Hz, whereas it becomes negligible for dihedral angles around 115° and somewhere between 45° and 60°. Close to the gauche conformation the differences become actually negative and go through a second maximum about 150°. We have to conclude therefore that the shape of the calculated Karplus curve depends on the method employed in the geometry optimization as can also be seen from the coefficients C_n in the Fourier series representation of the curves given in the Supporting Information.[50] From the last two columns in Table 3 we can see that for most dihedral angles the geometry induced changes are mainly due to the FC term, whereas around the gauche

Table 3: Calculated $^{3}J_{FF}$ Karplus Curves as a Function of the Method and Optimized Geometry Used in the Calculations[a]

	B3LYP-geometry		MP4-geometry					Δ MP4-B3LYP geometry[b]		
									SOPPA(CCSD)	
ϕ [°]	RAS-B J^{3Tot}_{FF}	SOPPA-(CCSD) J^{3Tot}_{FF}	RPA J^{3Tot}_{FF}	RAS-A J^{3Tot}_{FF}	RAS-B J^{3Tot}_{FF}	SOPPA J^{3Tot}_{FF}	SOPPA(CCSD) J^{3Tot}_{FF}	RAS-B J^{3Tot}_{FF}	$^{3}J^{FC}_{FF}$	J^{3Tot}_{FF}
0	36.50	30.28	54.16	44.11	38.03	32.98	31.84	1.53	1.23	1.56
15	30.05	24.60	46.16	37.29	31.49	26.93	26.07	1.44	1.13	1.47
30	14.30	10.98	26.17	20.46	15.65	12.50	12.31	1.35	1.17	1.33
45	−2.12	−2.58	3.13	1.56	−1.35	−2.36	−1.87	0.77	0.82	0.71
60	−10.71	−8.96	−12.46	−10.21	−10.85	−9.94	−9.12	−0.14	0.05	−0.16
80	−10.01	−8.25	−15.89	−11.52	−10.56	−9.51	−8.77	−0.55	−0.29	−0.52
90	−8.39	−7.78	−13.52	−9.71	−8.89	−8.94	−8.26	−0.50	−0.18	−0.48
100	−7.50	−8.57	−10.21	−7.99	−7.82	−9.60	−8.91	−0.32	0.01	−0.34
115	−7.66	−12.18	−4.10	−6.13	−7.61	−13.13	−12.21	0.05	0.36	−0.03
135	−10.22	−20.54	4.51	−5.46	−9.67	−21.74	−20.11	0.55	0.81	0.43
150	−13.07	−27.45	9.42	−6.43	−12.39	−29.17	−26.86	0.68	0.98	0.59
165	−14.95	−32.24	12.89	−7.30	−14.33	−34.49	−31.67	0.62	1.01	0.57
180	−16.69	−33.83	14.29	−7.56	−16.15	−36.35	−33.34	0.54	1.02	0.49

[a] Basis set: F and C, aug-cc-pVTZ-J; H, cc-pVTZ. [b] Difference between the $^{3}J_{FF}$ calculated at the geometries optimized with DFT-B3LYP and MP4 with the 6-311G(d,p) basis set.

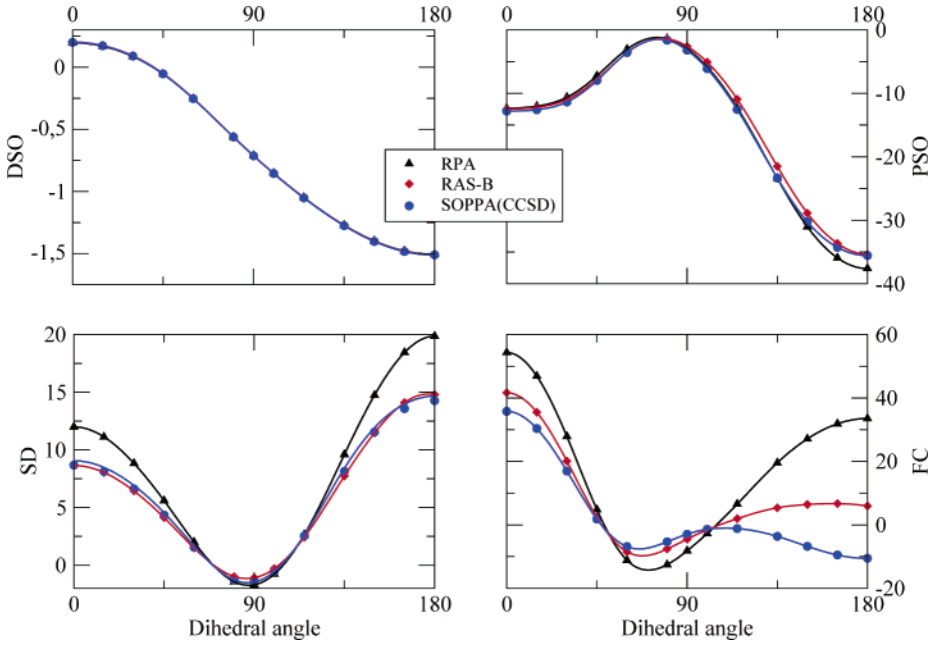

Figure 2. DSO, PSO, SD, and FC contributions to $^3J_{FF}$ at RPA, RAS-B, and SOPPA(CCSD) levels of approximation.

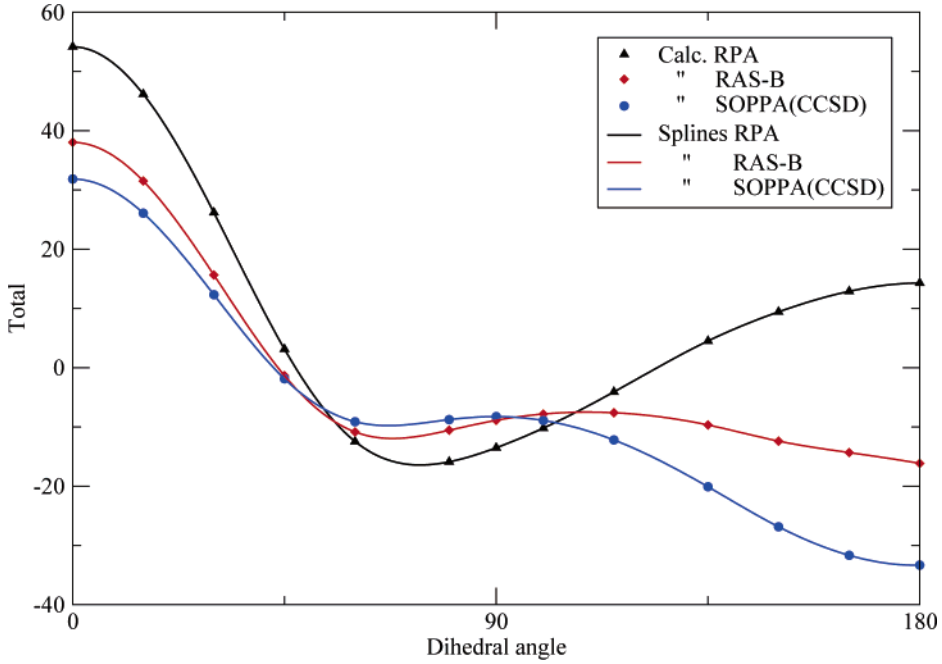

Figure 3. Total indirect nuclear spin−spin coupling constant $^3J_{FF}$ at RPA, RAS-B, and SOPPA(CCSD) levels of approximation.

conformation the smaller changes in the PSO term become dominant due to vanishing changes in the FC term.

4.3. Dependence of $^3J_{FF}$ on Electron Correlation. The total vicinal fluorine−fluorine coupling constants calculated with RPA, RAS-A MCRPA, RAS-B MCRPA, SOPPA, and SOPPA(CCSD) at the MP4 geometries are also presented in Table 3. The four contributions to $^3J_{FF}(\phi)$ and $^3J^{Tot}_{FF}(\phi)$ at the RPA, RAS-B MCRPA, and SOPPA(CCSD) levels are furthermore shown in Figures 2 and 3. Tables with all the results for both sets of geometries are available from the Supporting Information.[50]

It is a well-known fact[27,30,54,55] that the electron correlation is often irrelevant for the two singlet contributions, DSO and PSO, and very important for quantitative reproduction of the two triplet contributions, SD and FC, and thus for the total indirect coupling constant, if the FC term is the dominant contribution. It is therefore not surprising that all four contributions to $^3J_{FF}(\phi)$ exhibit a very different dependence on electron correlation as shown in Figure 2. The DSO term is completely insensitive to electron correlation, while the PSO term changes only slightly around the trans conformation, where the RPA method underestimates the SOPPA(CCSD) value of −35.55 Hz by 2.05 Hz, i.e. ∼5.8%.

Larger changes, on the other hand, are observed for the two triplet contributions SD and FC. The effect of electron correlation on the SD contribution is recovered similarly by the RAS-B MCRPA and SOPPA(CCSD) calculations for the whole range of conformations. RPA overestimates the SD

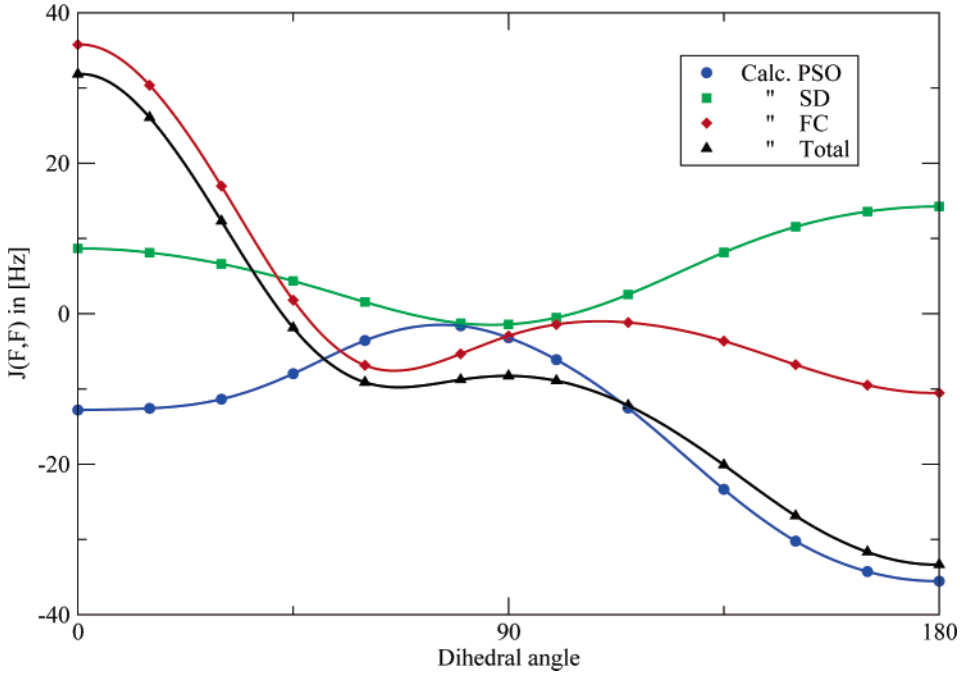

Figure 4. DSO, PSO, SD, and FC contributions to $^3J_{FF}$ at SOPPA(CCSD) level of approximation.

term compared to SOPPA(CCSD) and RAS-B MCRPA. The RPA values are about a factor of 1.3 too large. In absolute values this becomes most prominent for the cis and trans conformations, where the RAS-B MCRPA and SOPPA(CCSD) results differ from RPA by about 3.3 Hz for *cis*-1,2-difluoroethane and 5.6 Hz for *trans*-1,2-difluoroethane. However, it is important to point out that for all dihedral angles between 45° and 135° the deviation of the RPA results from SOPPA(CCSD) is smaller than 1.0 Hz. Hence, we can conclude that for most conformers of 1,2-difluoroethane the SD term is almost not affected by electron correlation.

The largest effect of the electron correlation can be observed for the FC contribution. It is changed for all values of the dihedral angle, but the changes for near-trans conformations are much larger than those for near-cis or near-gauche conformations. For the near-trans conformations, electron correlation reduces the FC term until it even changes sign. The corresponding changes in the FC term are as follows: ∼27.6 Hz from RPA (33.53 Hz) to RAS-B (5.94 Hz) and ∼16.5 Hz from RAS-B to SOPPA(CCSD) (−10.54 Hz). For *cis*-1,2-difluoroethane, on the other hand, the reduction in the FC term is less pronounced: 12.66 Hz from RPA (33.53 Hz) to RAS-B (5.94 Hz) and 5.88 Hz from RAS-B to SOPPA(CCSD) (35.76 Hz). Thus, the Karplus-like shape of the curve found at the RPA level of approximation is broken when the electron correlation is added in the calculation of the FC term.

Overall we find that the shape of the RAS-B MCRPA FC curve is more similar to the RPA curve than to the SOPPA curve. RAS-B overestimates also slightly the FC contribution around the cis and gauche conformations and predicts also the wrong sign of FC around the trans conformation. This holds even more for the RAS-A MCRPA curve. We observe thus a continuous change in the coupling constant curve on going from RPA through increasingly larger MCRPA calculations to SOPPA(CCSD), i.e. with a better and better description of dynamic correlation.

Noteworthy is the fact that the change in the sign of the FC contribution for the near-trans conformations at SOPPA(CCSD) level does not agree with the Dirac vector model,[56] which predicts a positive three bond FF coupling. Furthermore, around the gauche conformations the Dirac vector model is not fulfilled for all level of approximations.

4.4. Dependence of $^3J_{FF}$ on the Dihedral Angle. In Figures 2 and 4 one can see that all four contributions exhibit also a very different dependence on the dihedral angle. We can furthermore see that the total vicinal coupling constant is dominated by the FC contribution in the range of dihedral angles from the cis to the gauche conformation. The always negative PSO contribution is almost canceled by the positive SD contribution in this range leading to a shift of about −4 Hz with respect to the FC term. Within ±50 around the trans conformation, however, the total coupling constant is dominated by the PSO term, because here the positive SD contribution is almost compensated by the negative FC term, so that the curve is shifted by about 4 Hz compared to the PSO curve. This corresponds qualitatively to the findings by Kurtkaya et al.[7] although quantitatively their B3LYP curve differs greatly from our SOPPA(CCSD) curve.

The Fourier analysis according to eq 8 of the dihedral angle dependence of $^3J_{FF}$ shows that for all levels of calculation the first five coefficients are larger than 1 Hz and are necessary for fitting the curves, see Table 4. At the SOPPA(CCSD) level the FC contribution follows the same scheme as the total coupling constant, and five coefficients are also necessary to fit the FC curve as well. For the SD and PSO contributions, on the other hand, only the first three and the fifth coefficients are necessary for fitting the curves. This is very much in contrast to the vicinal proton−proton

Table 4: Coefficients of the Cosine Series (in Hz) of $^3J_{FF}$ in 1,2-Difluoroethane at Various Levels of Approximation

method	contribution	C_0	C_1	C_2	C_3	C_4	C_5	C_6	C_7
RPA	$^3J_{FF}^{Tot}$	6.999	9.702	24.204	10.118	3.277	0.318	−0.365	−0.279
RAS-A	$^3J_{FF}^{Tot}$	1.111	15.609	14.294	10.053	3.123	0.362	−0.335	−0.259
RAS-B	$^3J_{FF}^{Tot}$	−2.207	16.536	10.337	9.895	3.301	0.623	−0.393	−0.131
SOPPA	$^3J_{FF}^{Tot}$	−8.695	24.396	3.760	9.854	3.369	0.609	−0.160	−0.251
SOPPA(CCSD)	$^3J_{FF}^{Tot}$	−7.761	22.945	3.887	9.245	3.241	0.588	−0.155	−0.242
	$^3J_{FF}^{DSO}$	−0.675	0.859	0.028	−0.001	−0.010	−0.003	0.001	0.001
	$^3J_{FF}^{PSO}$	−14.610	11.170	−10.799	−0.049	0.981	0.312	0.318	−0.036
	$^3J_{FF}^{SD}$	5.615	−2.747	6.410	−0.144	−0.606	0.086	0.030	0.014
	$^3J_{FF}^{FC}$	1.909	13.664	8.248	9.440	2.876	0.193	−0.504	−0.221

Table 5: Calculated Gauche Angle and Corresponding $^3J_{FF}$ at RPA, RAS-B MCRPA, and SOPPA(CCSD) Levels[a]

geometry	angle [°]	level	J^{Total} [Hz]
DFT	71.683	RPA	−15.68
		RAS-B	−11.22
		SOPPA	−9.87
		SOPPA(CCSD)	−9.07
MP4	69.442	RPA	−16.10
		RAS-B	−11.96
		SOPPA	−10.59
		SOPPA(CCSD)	−9.77

[a] Values were obtained fitting the calculated curves using second degree splines.

couplings in ethane where only the three original Karplus coefficients are necessary (see e.g. ref 17).

4.5. Comparison with Previous Results. The couplings for the trans and gauche conformations have been estimated by Abraham and Kemp[53] to be −30 Hz and −10.9 Hz, respectively. Later on refs 51 and 52, the dihedral angle in the gauche conformation of 1,2-difluoroethane was estimated to be 71.0°−71.3°.

Using second degree splines to fit the calculated energy curves for the geometries optimized at the DFT-B3LYP and MP4 levels with the 6-311G(p,d) basis set, we found that the best estimate of the gauche angle is obtained at the DFT-B3LYP level with a value of ∼71.7°, Table 5, which agrees with the results reported by Kurtkaya et al.[7] of ∼72.0 Hz. However, the best estimate of the vicinal coupling in the gauche conformation occurs at the SOPPA level with a value of ∼10.6 Hz for the MP4-geometry, whereas RAS-B underestimates it and SOPPA(CCSD) overestimates it. Finally, for the trans conformation the best estimate comes from the SOPPA(CCSD) calculations which predicts ∼ −33.8 Hz for the DFT-geometry and ∼ −33.3 Hz for the MP4-geometry, whereas for this conformer SOPPA underestimates the coupling by −3.01 Hz and the RAS-B method overestimates it by 17.19 Hz.

The $^3J_{FF}(\phi)$ curve calculated at the DFT-D3LYP level by Kurtkaya et al.[7] and of course also the SOPPA curve by San Fabián and Westra Hoekzema[9] are similar to our SOPPA(CCSD) curve. However, the SOPPA(CCSD) couplings are smaller in absolute value than the DFT-D3LYP and SOPPA results. Previous experience with F−F coupling constant calculations[8,10] showed that the SOPPA(CCSD) results are in general in better agreement with experimental couplings than SOPPA results, as it is the case also for most other couplings studied so far[17,27,30−34] and for the Karplus curve of the vicinal proton−proton couplings in ethane.[17] We expect therefore that the SOPPA(CCSD) Karplus curve for the vicinal F−F couplings in 1,2-difluoroethane is also superior to a corresponding SOPPA curve. The largest differences between the SOPPA and SOPPA(CCSD) results are observed for the near-trans conformations with deviations of about 3.0 Hz in favor of the latter.

5. Summary

We have optimized the geometry of 1,2-difluoroethane for different dihedral angles ∠F−C−C−F at two levels of approximation, DFT-B3LYP and MP4, using the 6-311G-(p,d) basis set. The calculated energies were interpolated with second-order splines in order to obtain the dihedral angle of the gauche conformation. For every optimized geometry $^3J_{FF}$ was calculated at different levels of theory: RPA, MCRPA (RAS-A and RAS-B), SOPPA, and SOPPA(CCSD). The obtained coupling constant curves were fitted to Fourier cosine series.

We find that the form of the Karplus curve depends on the method chosen in the geometry optimization because the changes are largest for the cis conformation. With the exception of dihedral angles close to the gauche angle it is mostly the FC term which is influenced by the changes in the geometry.

Electron correlation affects also mostly the FC contribution. However, these changes are larger for near-trans conformations than for near-cis or near-gauche conformations. For the near-trans conformations even the sign of the FC term is changed by electron correlation. The SD contribution, on the other hand, is affected almost equally for all dihedral angles, and the DSO and PSO terms are almost not affected by electron correlation at all. Hence, one can attribute the capricious form of the F−F Karplus curve in 1,2-difluoroethane to electron correlation effects on the FC contribution.

For dihedral angles in the range from the cis to the gauche conformation the total vicinal coupling constant is dominated by the FC contribution, whereas around the trans conformation it is dominated by the PSO term.

Comparison with previous DFT-B3LYP and SOPPA calculations shows that these follow the same trend as our SOPPA(CCSD) curve. However, along the whole range of dihedral angles the SOPPA(CCSD) couplings are smaller in absolute values than the results of the other two methods by

∼10 Hz (in the cis conformation) to 25 Hz (in the trans conformation) for B3LYP[7] and by 1 Hz (in the cis conformation) to 3 Hz (in the trans conformation) for SOPPA calculations with the MP4 geometry of this work.

Finally we note that the positive value for $^3J_{FF}^{FC}$ predicted by the Dirac vector model is not reproduced by all our calculated values around the gauche conformations and at the SOPPA(CCSD) level already from dihedral angles from ∼45° on.

Acknowledgment. The authors want to thank Ruben H. Contreras, James P. Snyder, and their groups for providing us with the challenge of this project and the B3LYP molecular geometries. This research was supported financially by grants from SNF, FNU, and the Carlsberg Foundation and by computer time grants from DCSC. P.F.P. acknowledges support from CONICET and the CU-DNRC.

Supporting Information Available: Total energies of 1,2-difluoroethane as a function of the F-F dihedral angle obtained by geometry optimization at the HF, B3LYP, MP2, MP3, and MP4 levels; the four contributions to the vicinal F-F indirect nuclear spin−spin coupling constant at the RPA, RAS-A, RAS-B, SOPPA, and SOPPA(CCSD) levels as a function of the F-F dihedral angle for the B3LYP and MP4 optimized geometries; and Fourier coefficients of the dihedral angle dependence of the vicinal F-F indirect nuclear spin−spin coupling constant obtained at the SOPPA(CCSD) level for the B3LYP and MP4 optimized geometries are all given in the Supporting Information. This material is available free of charge via the Internet at http://pubs.acs.org.

References

(1) Contreras, R. H.; Peralta, J. E. *Prog. Nucl. Magn. Res. Spectrosc.* **2000**, *37*, 321−425.

(2) Karplus, M. *J. Chem. Phys.* **1959**, *30*, 11−15. Karplus, M. *J. Am. Chem. Soc.* **1963**, *85*, 2870−2871.

(3) Wilkens, S. J.; Westler, J. L.; Markley, J. L.; Weinhold, F. *J. Am. Chem. Soc.* **2001**, *123*, 12026−12036. Provasi, P. F.; Gómez, C. A.; Aucar, G. A. *J. Phys. Chem. A* **2004**, *108*, 6231−6238.

(4) Peruchena, N. M.; Aucar, G. A.; Contreras, R. H. *J. Mol. Struct. (THEOCHEM)* **1990**, *210*, 205−210. Lantto, P.; Kaski, J.; Vaara, J.; Jokisaari, J. *Chem. Eur. J.* **2000**, *6*, 1395−1406. Barone, V.; Peralta, J. E.; Contreras, R. H.; Snyder, J. P. *J. Phys. Chem. A* **2002**, *106*, 5607−5612.

(5) Peralta, J. E.; Barone, V.; Contreras, R. H.; Zaccari, D. G.; Snyder, J. P. *J. Am. Chem. Soc.* **2001**, *123*, 9162−9163.

(6) Lantto, P.; Vaara, J.; Helgaker, T. *J. Chem. Phys.* **2002**, *117*, 5998−6009.

(7) Kurtkaya, S.; Barone, V.; Peralta, J. E.; Contreras, R. H.; Snyder, J. P. *J. Am. Chem. Soc.* **2002**, *124*, 9702−9703.

(8) Barone, V.; Provasi, P. F.; Peralta, J. E.; Snyder, J. P.; Sauer, S. P. A.; Contreras, R. H. *J. Phys. Chem. A* **2003**, *107*, 4748−4754.

(9) San Fabián, J.; Westra Hoekzema, A. J. A. *J. Chem. Phys.* **2004**, *121*, 6268−6276.

(10) Provasi, P. F. Aucar, G. A.; Sauer, S. P. A. *J. Phys. Chem. A* **2004**, *108*, 5393−5398.

(11) Sanchez, M.; Provasi, P. F.; Aucar, G. A.; Sauer, S. P. A. *Adv. Quantum Chem.* **2005**, *48*, 161−183.

(12) Contreras, R. H.; Esteban, Á. L.; Della, N. J.; Díez, E. W.; Head, E. *Mol. Phys.* **2006**, *104*, 485−492.

(13) Feeney, J.; McCormick, J. E.; Dauer, C. J.; Birdsall, B.; Moody, C. M.; Starkmann, B. A.; Young, D. W.; Francis, P.; Havlin, R. H.; Arnold, W. D.; Oldfield, E. *J. Am. Chem. Soc.* **1996**, *118*, 8700−8706. Colmenares, L. U.; Zou, X.; Liu, J.; Asato, A. E.; Liu R. S. H. *J. Am. Chem. Soc.* **1999**, *121*, 5803−5804. Bilgiçer, B.; Fichera, A.; Kumar, K. *J. Am. Chem. Soc.* **2001**, *123*, 4393−4399. Bilgiçer, B.; Xing, X.; Kumar, K. *J. Am. Chem. Soc.* **2001**, *123*, 11815−11816. Duewel, H. S.; Daub, E.; Robinson, V.; Honek, J. F. *Biochemistry* **2001**, *40*, 13167−13176. Kitteringham, N. R.; O'Neill, P. M. Metabolism of fluorine-containing drugs. In *Annu. Rev. Pharmacol. Toxicol.* **2001**.

(14) Bachert, P. *Prog. Nucl. Magn. Res. Spectrosc.* **1998**, *33*, 1−56.

(15) Tei, M.; Mizuno, Y.; Manmoto, Y.; Sawae, R.; Takarabe, K. *Int. J. Quantum Chem.* **2003**, *95*, 554−557.

(16) Hirao, K.; Nakatsuji, H.; Kato, H.; Yonezawa, T. *J. Am. Chem. Soc.* **1972**, *94*, 4078−4087. Hirao, K.; Nakatsuji, H.; Kato, H. *J. Am. Chem. Soc.* **1973**, *95*, 31−41.

(17) Grayson, M.; Sauer, S. P. A. *Mol. Phys.* **2000**, *98*, 1981−1990.

(18) Helgaker, T.; Watson, M.; Handy, N. C. *J. Chem. Phys.* **2000**, *113*, 94022−9409.

(19) Hohenberg, P.; Kohn, W. *Phys. Rev.* **1964**, *136*, B864−B871. Kohn, W.; Sham, L. J. *Phys. Rev.* **1965**, *140*, A1133−A1138.

(20) Becke, A. D. *J. Chem. Phys.* **1993**, *98*, 5648−5652. Lee, C.; Yang, W.; Parr, R. G. *Phys. Rev. B* **1988**, *37*, 785−789. Miehlich, B.; Savin, A.; Stoll, H.; Preuss, H. *Chem. Phys. Lett.* **1989**, *157*, 200−206.

(21) Pople, J. A.; Hehre, W. J.; Ditchfield. R. *J. Chem. Phys.* **1972**, *56*, 2257−2261. Clark, T.; Chandrasekhar, J.; Spitznagel, G. W.; Schleyer, P. V. R. *J. Comput. Chem.* **1983**, *4*, 294−301.

(22) Malkin, V. G.; Malkina, O. L.; Salahub, D. R. *Chem. Phys. Lett.* **1994**, *221*, 91−99. Malkina, O. L. Salahub, D. R.; Malkin, V. G. *J. Chem. Phys.* **1996**, *105*, 8793−8800.

(23) Dalgaard, E.; Jørgensen, P. *J. Chem. Phys.* **1978**, *69*, 3833−3844. Yeager, D. L.; Jørgensen, P. *J. Chem. Phys.* **1979**, *71*, 755−760. Yeager, D. L.; Jørgensen, P. *Chem Phys. Lett.* **1979**, *65*, 77−80. Vahtras, O.; Ågren, H.; Jørgensen, P.; Aa. Jensen, H. J.; Padkjær, S. B.; Helgaker, T. *J. Chem. Phys.* **1992**, *96*, 6120−6125.

(24) Olsen, J.; Jørgensen, P. *J. Chem. Phys.* **1985**, *82*, 3235−3264.

(25) Olsen, J.; Roos, B. O.; Jørgensen, P.; Aa. Jensen, H. J. *J. Chem. Phys.* **1988**, *89*, 2185−2192. Malmqvist, P.-Å.; Roos, B. O. *Chem. Phys. Lett.* **1989**, *245*, 189−193.

(26) Nielsen, E. S.; Jørgensen, P.; Oddershede, J. *J. Chem. Phys.* **1980**, *73*, 6238−6246. Packer, M. J.; Dalskov, E. K.; Enevoldsen, T.; Aa, J. H. J.; Oddershede, J. *J. Chem. Phys.* **1996**, *105*, 5886−5900. Bak, K. L.; Koch, H.; Oddershede, J.; Christiansen, O.; Sauer, S. P. A. *J. Chem. Phys.* **2000**, *112*, 4173−4185.

(27) Enevoldsen, T.; Oddershede, J.; Sauer, S. P. A. *Theor. Chem. Acc.* **1998**, *100*, 275−284.

(28) Dunning, T. H., Jr. *J. Chem. Phys.* **1989**, *90*, 1007−1023.

(29) Sauer, S. P. A. *J. Phys. B: At., Mol. Opt. Phys.* **1997**, *30*, 3773−3780.

(30) Kirpekar, S.; Sauer, S. P. A. *Theor. Chem. Acc.* **1999**, *103*, 146−153.

(31) Provasi, P. F. Aucar, G. A.; Sauer, S. P. A. *J. Chem. Phys.* **2001**, *115*, 1324−1334.

(32) Sauer, S. P. A.; Raynes, W. T.; Nicholls, R. A. *J. Chem. Phys.* **2001**, *115*, 5994−6006.

(33) Krivdin, L. B.; Sauer, S. P. A.; Peralta, J. E.; Contreras, R. H. *Magn. Reson. Chem.* **2002**, *40*, 187−194. Sauer, S. P. A.; Krivdin, L. B. *Magn. Reson. Chem.* **2004**, *42*, 671−686.

(34) Wigglesworth, R. D.; Raynes, W. T.; Sauer, S. P. A.; Oddershede, J. *Mol. Phys.* **1997**, *92*, 77−88. Wigglesworth, R. D.; Raynes, W. T.; Sauer, S. P. A.; Oddershede, J. *Mol. Phys.* **1998**, *94*, 851−862. Wigglesworth, R. D.; Raynes, W. T.; Kirpekar, S.; Oddershede, J.; Sauer, S. P. A. *J. Chem. Phys.* **2000**, *112*, 3735−3746. Wigglesworth, R. D.; Raynes, W. T.; Kirpekar, S.; Oddershede, J.; Sauer, S. P. A. *J. Chem. Phys.* **2001**, *114*, 9192.

(35) Krishnan, R.; Pople, J. A. *Int. J. Quantum Chem.* **1978**, *14*, 91−100. Krishnan, R. Frisch, M. J.; Pople, J. A. *J. Chem. Phys.* **1980**, *72*, 4244−4245.

(36) Rowe, D. J. *Rev. Mod. Phys.* **1968**, *40*, 153−166.

(37) Ramsey, N. F. *Phys. Rev.* **1953**, *91*, 303−307.

(38) Sauer, S. P. A. *J. Chem. Phys.* **1993**, *98*, 9220−9221.

(39) Mills, I. Cvitas, T.; Homann, K.; Kallay, N.; Kuchitsu, K. *Quantities Units and Symbols in Physical Chemistry*; Blackwell Scientific: Oxford, 1993.

(40) Linderberg, J.; Öhrn, Y. *Propagator in Quantum Chemistry*; Acadamic Press: New York, 1973. Jørgensen, P.; Simons, J. *Second Quantization-Based Methods in Quantum Chemistry*; Academic Press: 1981.

(41) Sauer, S. P. A.; Packer, M. J. *In Computational Molecular Spectroscopy*; Bunker, P. R., Jensen, P., Eds.; Wiley: London, 2000.

(42) Møller, C.; Plesset, M. S. *Phys. Rev.* **1934**, *46*, 618−622.

(43) Oddershede, J.; Jørgensen, P. *J. Chem Phys.* **1977**, *66*, 1541−1556.

(44) Hansen, Aa. E.; Bouman, T. D. *Mol. Phys.* **1979**, *37*, 1713−1724.

(45) Parkinson, W. A.; Sabin, J. R.; Oddershede, J. *Theor. Chem. Acta* **1993**, *86*, 167−179.

(46) Frisch, M. J.; Trucks, G. W.; Schlegel, H. B.; Scuseria, G. E.; Robb, M. A.; Cheeseman, J. R.; Zakrzewski, V. G.; Montgomery, J. A., Jr.; Stratmann, R. E.; Burant, J. C.; Dapprich, S.; Millam, J. M.; Daniels, A. D.; Kudin, K. N.; Strain, M. C.; Farkas, O.; Tomasi, J.; Barone, V.; Mennucci, B.; Cossi, M.; Adamo, C.; Jaramillo, J.; Cammi, R.; Pomelli, C.; Ochterski, J.; Petersson, G. A.; Ayala, P. Y.; Morokuma, K.; Malick, D. K.; Rabuck, A. D.; Raghavachari, K.; Foresman, J. B.; Ortiz, J. V.; Cui, Q.; Baboul, A. G.; Clifford, S.; Cioslowski, J.; Stefanov, B. B.; Liu, G.; Liashenko, A.; Piskorz, P.; Komaromi, I.; Gomperts, R.; Martin, R. L.; Fox, D. J.; Keith, T.; Al-Laham, M. A.; Peng, C. Y.; Nanayakkara, A.; Challacombe, M.; Gill, P. M. W.; Johnson, B.; Chen, W.; Wong, M. W.; Andres, J. L.: Gonzalez, C.; Head-Gordon, M.; Replogle, E. S.; Pople, J. A. *Gaussian98, Revision A.11.2. Development Version, revision C.01*; Gaussian, Inc.: Pittsburgh, PA, 2001.

(47) Helgaker, T.; Jensen, H. J. Aa.; Jørgensen, P.; Olsen, J.; Ruud, K.; Ågren, H.; Auer, A. A.; Bak, K. L.; Bakken, V.; Christiansen, O.; Coriani, S.; Dahle, P.; Dalskov, E. K.; Enevoldsen, T.; Fernandez, B.; Heattig, C.; Hald, K.; Halkier, A.; Heiberg, H.; Hettema, H.; Jonsson, D.; Kirpekar, S.; Kobayashi, R.; Koch, H.; Mikkelsen, K. V.; Norman, P.; Packer, M. J.; Saue, T.; Sauer, S. P. A.; Taylor, P. R.; Vahtras, O. *DALTON, an electronic structure program, Release 1.2*; http://www.kjemi.uio.no/software/dalton/dalton.html, 2001.

(48) Provasi, P. F.; Aucar, G. A.; Sauer, S. P. A. *J. Chem. Phys.* **2000**, *112*, 6201−6208.

(49) The aug-cc-pVTZ-J basis set can be found at http://fyskem.ki.ku.dk/sauer/basissets.

(50) See the Supporting Information.

(51) Friesen, D.; Hedberg, K. *J. Am. Chem. Soc.* **1980**, *102*, 3987−3994.

(52) Takeo, H. Matsumura, C.; Morino, Y. *J. Chem. Phys.* **1986**, *84*, 4205−4210.

(53) Abraham, R. J.; Kemp, R. H. *J. Chem. Soc. B* **1971**, 1240−1245.

(54) Scuseria, G. E. *Chem. Phys. Lett.* **1986**, *127*, 236−241.

(55) Helgaker, T. Jaszunski, M.; Ruud, K. *Chem. Rev.* **1999**, *99*, 293−352.

(56) Harris, R. K. *Nuclear Magnetic Resonance Spectroscopy*; Pitman-London: 1983.

CT6000973